



APPLICATIONS-DESIGN OF BUCKLING RESTRAINED BRACES IN JAPAN

Mamoru IWATA¹

SUMMARY

Four commercially available buckling restrained braces are tested and evaluated. The different buckling restrained braces are prepared under the same conditions so that they cause no buckling and exhibit sufficient hysteresis even when they are subjected to a large earthquake with a story deformation angle of 1/100. The hysteresis characteristics and final fracture characteristics of the buckling restrained braces are determined by experiments, and the cumulative absorbed energy by them is calculated. Then, the author performs numerical analyses based on input different levels of ground motions. The performance of buckling restrained braces is evaluated using the data obtained from the comparative performance tests.

INTRODUCTION

The buckling restrained brace is a brace whose core plate is covered with a restraining part to prevent buckling. An unbonded material or a clearance is provided between the core plate and restraining part so that the axial force borne by the core plate is not transmitted to the restraining part (Figure 1). Theoretically, a buckling restrained brace does not buckle if the maximum compressive force arising in the core plate remains smaller than the Euler's buckling load of the restraining part. The buckling restrained brace produces equal yield strengths against both tensile and compressive forces and ensures a stable hysteresis.

A design method that is becoming increasingly popular in Japan keeps columns and beams of buildings in elastic regions as much as possible by using buckling restrained braces as hysteretic dampers. According to this design method, called damage-controlled structure (Wada [1]), buckling-restrained braces plasticize to provide hysteresis damping when medium earthquake occurs, thereby keeping columns and beams in elastic regions when large earthquake occurs.

This significantly reduces the plastic strain of connections of columns and beams, and keeps them undamaged, even when shaken by incredible large earthquakes. The damage-controlled structure has several economic advantages over conventional methods that include weight saving throughout the whole structure of a building, confining the need for after-earthquake inspection, repair and replacement to buckling restrained braces, and permitting continued use of whole building.

¹ Professor, Kanagawa University

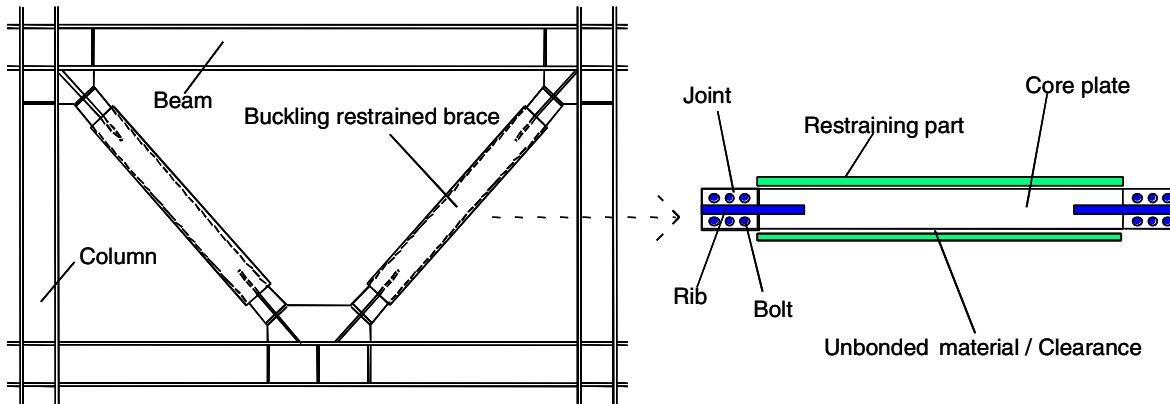


Figure 1. Buckling restrained brace

PURPOSE OF THE STUDY

The study aims at evaluating the critical-state performance of buckling restrained braces used as hysteretic dampers. Various methods to impose buckling restraint on braces have been conceived and tested. However, such methods do not allow direct comparison because sizes and types of specimens and testing methods employed are not the same. In this study, four commercially available buckling restrained braces are tested and evaluated. To make equal the yield strength of braces, the sectional area and length of core plates are equalized. Restraining parts are designed to have an equal geometrical moment of inertia that is used as a variable in imposing buckling restraint. The four different buckling restrained braces are prepared under the same conditions so that they cause no buckling and exhibit sufficient hysteresis even when they are subjected to a large earthquake in which the maximum ground motion of 0.5 m/s with a story deformation angle of 1/100. The hysteresis characteristics and final fracture characteristics of the individual buckling restrained braces are determined by experiments and the cumulative absorbed energy by them is calculated.

The extent, however, to which such braces, when incorporated in actual buildings, offer the performance that they were designed for is unknown. There are not any past studies that focused attention on the performance of such buckling strained braces while taking into account extremely rare levels of earthquake ground motions. The damage-controlled structure should be designed to allow some yielding of the primary structure in order to cope with such extremely rare instances.

This study identifies primary structure damage as well as the performance criteria for the buckling restrained brace. In order to achieve this end, using a damage-controlled structure model considered to be the most typical model, the author performs numerical analyses based on a highly-detailed frame analytical theory, and input different levels of ground motions. They also evaluate the performance of the buckling restrained braces using the data obtained from the comparative performance tests.

EXPERIMENT PROGRAM

Test specimens

Four types of specimens of the buckling restrained braces, Types 1, 2, 3 and 4 are prepared. Types 1, 2 and 3 have a core plate PL-16 x 176, whereas Type 4 has a core plate BH-136 x 136 x 9 x 6. The core plates are designed to have substantially the same sectional area. The core plates are made of the SN400B steel for building structures. This steel has good weldability and impact properties, with the upper and lower limits of yield point defined. The yield stresses measured in the test are 262.6 N/mm² for Types 1, 2

and 3 and 289.1 N/mm² for Type 4. The restraining parts are made of the STKR400 and SS400 steels, with their geometrical moment of inertia being designed to become substantially equal. Both ends of the core plates protruding from the restraining parts are cruciform-shaped to prevent the occurrence of local buckling.

Tables 1, 2 and 3 show a list of specimens used, their theoretical yield strengths and their material properties.

Table 1. Test specimens

Specimen	Core plate		Restraining part		
	Size (mm)	Sectional area (mm ²)	Size (mm)	Sectional area (mm ²)	Geometrical moment of inertia x10 ⁴ (mm ⁴)
Type 1	PL-16x176	2816	RP-210x150x3.2	2263	1114 Mortar (250)
Type 2	PL-16x176	2816	RP-150x150x6	3366	1150
Type 3	PL-16x176	2816	2C-180x75x7x10.5	7360	1171
Type 4	BH-136x136x9x6	2748	RP-150x150x6	3456	1196

Table 2. Calculated strength

Specimen	Core plate		Restraining part	P _E /P _y
	Yield load P _y (kN)	Yield strain (%)	Buckling load P _E (kN)	
Type 1	739.5	0.128	8939	12.1
Type 2	739.5	0.128	9228	12.5
Type 3	739.5	0.128	9396	12.7
Type 4	794.4	0.140	9597	12.1

Table 3. Material properties

Specimen	Yield stress (N/mm ²)	Tensile strength (N/mm ²)	Yield ratio (%)	Elongation (%)
Type 1	262.6	432.5	61	32
Type 2	262.6	432.5	61	32
Type 3	262.6	432.5	61	32
Type 4	289.1	451.3	64	29

Specimen Type 1

This specimen comprises a core plate covered with a rectangular hollow section that serves as a restraining part, with mortar filled in between the core plate and hollow section. An unbonded soft-rubber sheet (1 mm in thickness) is provided between the core plate and mortar (Figure 2(a)). The author designed and prepared this specimen based on the description in the reference (Fujimoto [2]).

Specimen Type 2

This specimen comprises a core plate that is covered with a rectangular hollow section alone (1 mm in clearance). No other restraining part and material is used (Figure 2(b)). The author designed this specimen based on the description in the reference (Kamiya [3]) and prepared under the same conditions that were employed in the preparation of Specimen Type 1.

Specimen Type 3

This specimen comprises a core plate that is covered with a restraining part that is formed by joining together the channel and flat steels with high-strength bolts. An unbonded soft-rubber sheet (1 mm in thickness) is provided between the core plate and restraining part (Figure 2(c)). The author designed this specimen based on the description in the reference (Fukuda [4]) and prepared under the same conditions that were employed in the preparation of Specimen Type 1.

Specimen Type 4

This specimen comprises a core plate consisting, unlike the core plate of other specimens, of a built-up wide-flange beam that is covered with a rectangular hollow section serving as a restraining part. A clearance of 1 mm is left between the core plate and rectangular hollow section, with no unbonded material filled (Figure 2(d)). The author designed this specimen based on the description in the reference (Suzuki [5]) and prepared under the same conditions that were employed in the preparation of Specimen Type 1.

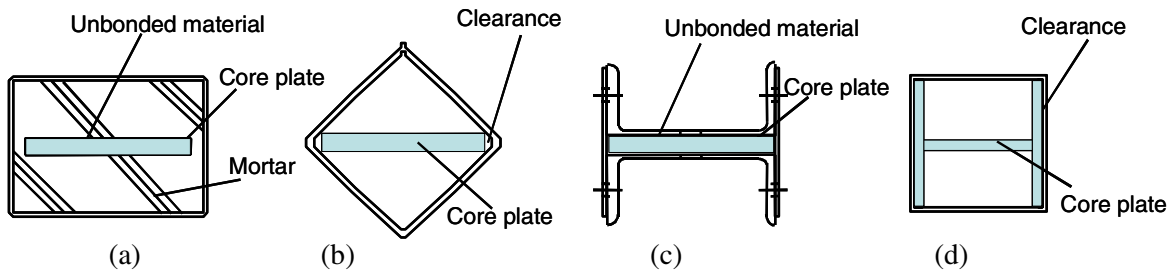


Figure 2. Section of specimens

Loading Method

A loading test machine (an electrically powered hydraulic actuator) is used for the application of load. Figure 3 shows the test equipment used in the experiment. The lower part of the H-400x400x13x21 jig is pin-supported.

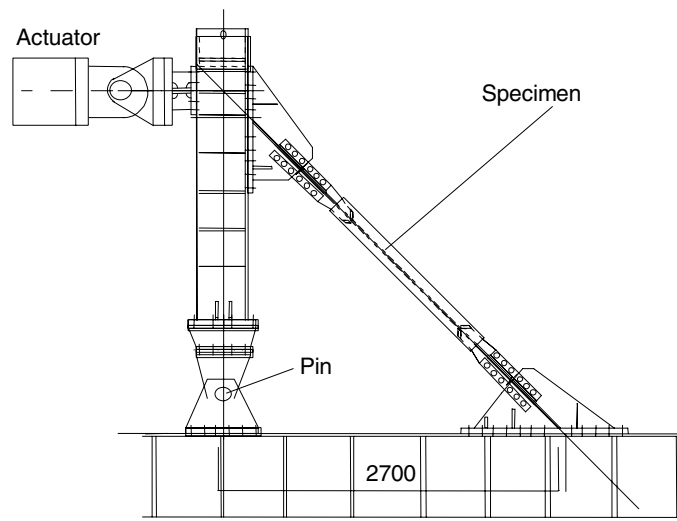


Figure 3. Loading test machine

Now that the specimen is placed in the direction of 45 degrees, the axial force developing in the specimen is square root of 2 times greater than the horizontal force from the actuator. The expansion and contraction of the specimen is one over square root of 2 greater than its horizontal deformation. The length of the specimen is square root of 2 times greater than the story height. Therefore, the axial strain arising in the specimen is one half the story deformation angle. However, the plastic strain occurring in the specimen becomes substantially equal to the story deformation angle. Because, the length of a portion of the specimen that undergoes plastic deformation is one half its overall length.

The strain of the specimen corresponding to a story deformation angle $1/200$ in a medium earthquake (in which the maximum ground motion of 0.25 m/s is 0.5 percent). The strain of the specimen corresponding to a story deformation angle $1/100$ in a large earthquake (in which the maximum ground motion of 0.5 m/s) is 1.0 percent. It is considered that buckling restrained braces must have a capacity to maintain a strain of up to 1.0 percent. And, then, tests are conducted with strains between 1.0 percent and 3.0 percent, which is equivalent to a story deformation angle 0.03 radian to determine critical-state performance.

Tests are conducted by applying increasing loads that are applied alternately in positive and negative directions (tension and compression). Control is exercised by varying load until the elastic region is reached and, then, by changing the axial deformation of the core plate beyond that region. One each load equal to $1/3$ and $2/3$ of the yield strain is applied before yielding. After yielding, tests are made with a 0.25 percent strain (once), 0.5 and 0.75 percent strains (twice each), 1.0 percent strain (five times), and 1.5, 2.0 and 2.5 percent strains (twice each). Then, a 3.0 percent strain is applied until strength dropped or the specimen fractured. Each load after yielding is applied twice (except 0.25 and 1.0 percent) to determine the stability of the loop.

EXPERIMENTAL RESULTS

Specimen Type 1

Loading was continued until the 14th application of a 3.0 percent strain (Figure 4(a)).

On the 14th compression with a 3.0 percent strain, the upper mortar collapsed under pressure and local buckling occurred in the core plate in the vicinity of the rib end. While the local buckling proceeded until the mortar ultimately collapsed under pressure, stable hysteresis was observed in both tension and compression. Maximum strength was 1,155 kN in tension and 1,296 kN in compression.

When the rectangular hollow section and mortar were removed, the exposed core plate exhibited a sign of high degree buckling mode.

Specimen Type 2

Loading was continued until the first application of a 2.5 percent strain (Figure 4(b)).

On the second compression with a 1.0 percent strain, local buckling occurred in an area slightly above the middle of the core plate. On the fifth compression with a 1.0 percent strain, the local buckling in the area slightly above the middle of the core plate proceeded and the rectangular hollow section was deformed. On the first tension with a 2.5 percent strain, the core plate near the upper rib end fractured. The maximum strength was 850 kN in tension and 806 kN in compression.

The core plate exhibited a sign of light buckling throughout, in addition to the area where local buckling proceeded. The rectangular hollow section used as a restraining part underwent a substantial cross-sectional deformation near the point of local buckling in the core plate. Cracks were observed in the same region.

Specimen Type 3

Loading was continued until the first application of a 3.0 percent strain (Figure 4(c)).

Sufficiently stable hysteresis was observed up to the application of a 1.0 percent strain. Local buckling started near the rib end on the first compression with a 2.5 percent strain and the clearance between the restraining part and core plate increased. Even then, hysteresis was substantially stable. On the first compression with a 3.0 percent strain, a shear fracture occurred in the high-strength bolts fastening the restraining part near the rib end. The maximum strength was 1,084 kN in tension and 1,078 kN in compression.

The core plate exhibited a sign of high degree buckling mode, in addition to the area where severe local buckling occurred.

Specimen Type 4

Loading was continued until the second application of a 2.5 percent strain (Figure 4(d)).

Hysteresis was sufficiently stable up to the application of a 1.0 percent strain, and remained substantially stable up to a 2.0 percent strain. On the second compression with a 2.0 percent strain, local buckling occurred in a region slightly below the middle of the core plate leading to the development of cracks in the rectangular hollow section. Then, local buckling in the flange of the core plate resulted in the bulging of the rectangular hollow section. On the first compression with a 2.5 percent strain, the local buckling slightly below the middle of the core plate proceeded and the cracks in the rectangular hollow section expanded and propagated to the opposite side of the section. Then, the web of the core plate bulged greatly downward along the weak axis as a result of local buckling. On the second tension with a 2.5 percent strain, the core plate fractured at a point slightly below the middle. The maximum strength was 1,169 kN in tension and 1,076 kN in compression.

The core plate exhibited a sign of high degree buckling mode in the flange, whereas no sign of deformation was observed in the web except at the fractured point. Some cracks were observed in the flange of the core plate.

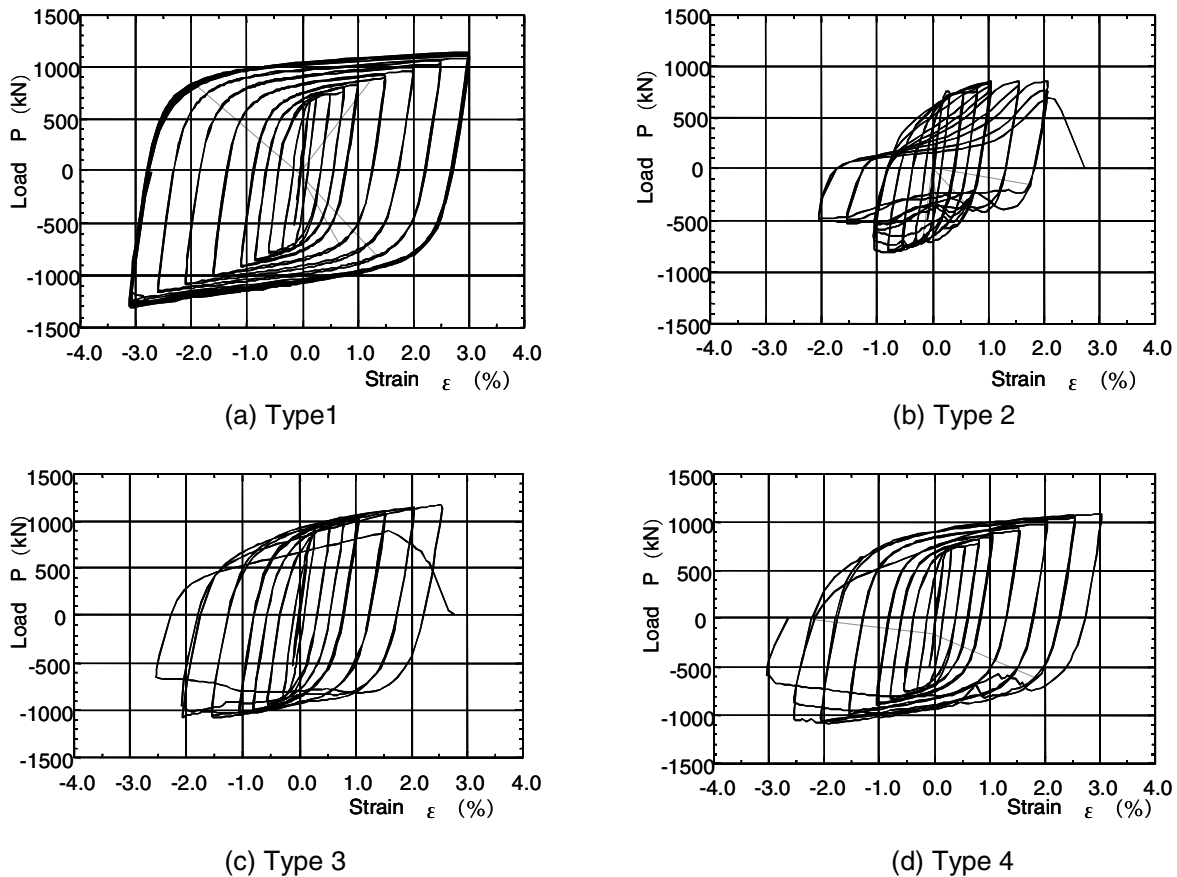


Figure 4. Load-Strain relations

DISCUSSIONS FOR THE RESULTS

Hysteresis characteristics

Substantially stable hysteresis was observed up to a 1.0 percent strain in all specimens.

Under high strains, all specimens but Type 1 exhibited a trough of load in compression. This is due to the local buckling of the core plate that proceeds to the extent allowed by the clearance between the core plate and the restraining part, thus causing a temporary drop in load. When the core plate comes in touch with the restraining part and deformation stops, load resumes its former course of rising. The degree of buckling mode rises by repeating this cycle. Thus, the core plates tested exhibited a sign of high degree buckling mode. In all specimens, a drop in strength started in a loop following the appearance of the trough of load. Therefore it can be said the deformation of the core plate becomes larger with an increase in the number of the trough of load, which, in turn, accelerates decline in strength.

Final fracture characteristics

Local buckling or tensile fracture occurred near the rib end in all specimens but Type 4. Specimen Type 4 also fractured, but, unlike other specimens, between the rib end and the center of the core plate. In Specimen Type 1, the mortar in the upper portion collapsed under pressure and local buckling occurred in the core plate near the rib end. It was only Specimens Type 2 and 4 that fractured in the test. The tensile fracture of Specimens Type 2 and 4 is considered to be ascribable to the absence of the unbonded material that prevented sufficient restraining of local buckling and allowed continued progress of plastic deformation. In Specimen Type 3, the high-strength bolts fastening together the channel and flat steels constituting a restraining part fractured by the action of shear force resulting from the progress of local buckling in the core plate.

Cumulative absorbed energy

The cumulative energies absorbed by the individual specimens throughout the test are as follows:

- (1) Specimen Type 1: 2,632 kN•m
- (2) Specimen Type 2: 292 kN•m
- (3) Specimen Type 3: 752 kN•m
- (4) Specimen Type 4: 617 kN•m

Specimen Type 1 that allowed applying a 3.0 percent strain fourteen times absorbed a much greater amount of energy than the other specimens. Specimens Type 2 and 4 fractured in the first and second tension with a 2.5 percent strain. Although the difference was only one cycle, Specimen Type 4 absorbed more than twice as much energy than Specimen Type 2. This result demonstrates that Specimen Type 2 did not exhibit good hysteresis under high strain.

NUMERICAL ANALYSIS METHOD

Design criteria for the damage-controlled structure

An example of design criteria for structures is provided in Table 4.

Table 4. An example of design criteria

In put energy (Level)		1	2	3	4	
Rank	S	Stress	Elastic	Elastic	Elastic	Elastic
		Deformation	1/300	1/200	1/150	1/100
	A	Stress	Elastic	Elastic	Elastic	Plastic
		Deformation	1/200	1/150	1/100	1/75
	B	Stress	Elastic	Elastic	Plastic	Plastic
		Deformation	1/150	1/100	1/75	1/50
	C	Stress	Elastic	Plastic	Plastic	Plastic
		Deformation	1/100	1/75	1/50	1/33

The structures are ranked S, A, B, and C in order of their performance. A frame built for the purpose of numerical analysis is designed to have a structural rank midway between A and B given the feature of the damage-controlled structure. This means that even if the sectional areas of the primary structural elements are reduced, the story deformation angle, when subjected to external forces equivalent in magnitude to seismic ground motions of high intensity, can be suppressed below 1/100 by maximizing the damper's energy absorption capability.

Settings for the analytical model

In the setting of the building frame to be established as the damage-controlled structure, the number of stories of the building is set at ten given that shear deformation predominates to maximize the effect of the dampers of the buckling restrained brace as well as to suppress the overall bending deflection due to column expansion/contraction to a negligible level. As for the number of spans, since K-form bracing was used for the testing, three spans with a bracing section placed in the center are considered to be the minimum required to achieve symmetry and a balance of stiffness with the frame. Based on the abovementioned conditions and the structural performance of the buckling restrained brace, this study considers a 10-story 3-span two-dimensional frame. The cross-sectional area of each structural member on each story is determined based on the condition that the story shear coefficient at the yield point on the first story (D_s) is 0.3. The ratio ($2K_b/K_f$) of the stiffness of the buckling restrained brace (K_b) to that of the primary structure (K_f) can be set within a range between 1.0 and 4.0. Response acceleration tends to increase, however, when the ratio exceeds 2.0. Response displacement also tends to increase when the ratio is below 2.0. For this reason, the ratio is set at 2.0 for all stories. The story shear at the damper yield point on each story Q_{dy} is set approximately at 1/10 of the horizontal load-carrying capacity of each story Q_{un} . Such a 10-story, 3-span analytical model is universal considering that most office buildings are more or less like this. In terms of the universality of numerical values, it is considered that, even if different frame types are used, universal results can be obtained from damper performance analysis if rigidity distribution, natural period, and criteria settings are equivalent to those adopted for the analytical model.

The analytical model design

The analytical model is designed to have a fixed column base with a 3.8 meter story height for the first story and 3.0 meters for the other stories. The beam span is set at 6.0 meters. Square steel pipes are used for columns, and wide flanges (yield stress: 323.4 N/mm²) for beams.

The buckling restrained brace consists of a damper unit and a gusset unit (hereinafter referred to as the damper and the gusset). The brace is positioned in the central span of the analytical model so as to form a K in each story. The damper (yield stress: 235.2 N/mm²) which uses a flat steel bar, is designed to have a plastic deformation region equivalent to half the overall brace length. The gusset (yield stress: 235.2 N/mm²) is modeled to have a cross-sectional area ten times larger than that of the damper. The damper is free from bending deflection in order to achieve conformity with the buckling restraining conditions. As for the weight design of the analytical model, one-fourth of the total story weight is distributed to each column-beam node, and one-tenth to the beam center. The weight of each story is approximated based on the assumption that the beam weight per meter is 39.2 kN, except for the 10th story which is 1/2 of the other stories. The external force distribution to be adopted in static incremental analysis shall be in accordance with the A_i distribution given in the Building Standard Law & the Building Standard Law Enforcement Order as well as in the notification by the Ministry of Land, Infrastructure and Transport in Japan. Table 5 shows the cross-sectional areas of the individual elements of the analytical model.

Analytical theory

In this study, analysis is performed using a non-linear one-dimensional frame dynamic response analysis program based on the Finite Element Method. Given below are the basic hypothetical conditions and theories (Fuimoto [6]).

(a) All the members are treated as linear elements.

- (b) Each member is divided into three smaller elements in the member direction. Each member is also divided into 20 layered elements in the cross-sectional direction.
- (c) The stress and strain distributions within the cross-section are constant in each divided element.
- (d) For each divided element, a polynomial equation is established that has a direct incremental displacement function in the direction of the member, and a tertiary incremental displacement function in the direction of the normal line, as opposed to the member direction.
- (e) Non-linear analysis is an incremental method based on the principle of stationary potential energy.
- (f) Time history response analysis is performed with an analytical program created based on Newmark's β -method ($\beta = 1/4$) and by using direct integration.

Table 5. Members of analytical model

Story	Column	Beam	Damper	$2K_b/K_f$	Q_{dy}/Q_{un}
10	250x6	240x170	9x25	2.1	0.12
9	350x8	300x200	12x32	1.9	0.10
8	350x9	340x250	12x45	2.0	0.10
7	350x11	360x300	12x60	2.1	0.11
6	400x11	390x300	12x70	2.0	0.10
5	400x12	390x300	12x80	2.1	0.11
4	400x12	390x300	12x85	2.0	0.10
3	400x14	440x300	12x90	1.9	0.10
2	400x14	440x300	12x95	1.9	0.10
1	400x15	440x300	16x110	1.9	0.13

Analytical conditions

The following analytical conditions have been established.

- (a) Young's modulus of steel is set at 205 kN/mm². Plasticity gradient is 1/50 of Young's modulus, and the coefficient that considers strain hardening is 1/200 of Young's modulus.
- (b) Damping is time-dependent and proportional to stiffness, and the damping ratio corresponding to the first-order natural period is 2%.
- (c) The earthquake ground motion records adopted are El Centro NS (elns), Kobe Marine Observatory NS (kobens), Taft EW (taftew), and Hachinohe EW (hatiew). The simulated earthquake ground motion records created and released by the Building Center of Japan (center) are also used.
- (d) In earthquake ground motion level settings, level-1 and level-2 ground motions are those considered during the general design operations. Level-3 and level-4 ground motions are intended to be used for safety margin assessment to determine the damper's limit-state performance.
- (e) The observed ground motion records are normalized into four peak velocity levels of 0.25 m/s, 0.5 m/s, 0.75 m/s, and 1.0 m/s. With the simulated ground motion records, level-3 and level-4 ground motions are created in which the accelerations of the former and the latter are 1.5 times and 2 times, respectively, that of level-2 ground motion. Table 6 shows the peak ground motion accelerations of the individual ground motions adopted. (The abbreviations of the individual ground motions are also used in Tables 7, 8, 9, and 10 along with their levels, L1, L2, L3, and L4.)

Table 6. Peak ground motion accelerations Unit (m/s²)

Ground motion	L1 (Level-1)	L2 (Level-2)	L3 (Level-3)	L4 (level-4)
El centro NS: elns	2.42	4.84	7.26	9.68
Kobe NS: kobens	2.23	4.47	6.71	8.93
Taft EW: taftew	2.43	4.87	7.30	9.74
Hachinohe EW: hatiew	1.21	2.41	3.62	4.82
Center: center	2.07	3.56	5.33	7.11

Eigenvalue analysis

It was found from the results of eigenvalue analysis using initial stiffness that the first-order natural period is 1.1 seconds and the second-order natural period is 0.4 seconds. The first- and second-order natural periods of the primary structural elements without bracing are 1.7 seconds and 0.6 seconds, respectively.

ANALYTICAL RESULTS

Maximum responses to different levels of ground motion inputs

Figure 5 shows the maximum story deformation angle distribution. This set of data is presented as an illustrative example of the analytical results obtained from the “kobens” (Kobe Marine Observatory NS) that exhibited relatively large responses to the ground motion inputs from level-1 to level-4 adopted in this study. The story deformation angle in the analytical model is found to be approximately 1/200, 1/100, 1/75, and 1/50, respectively, at the level-1, level-2, level-3 and level-4 ground motion inputs.

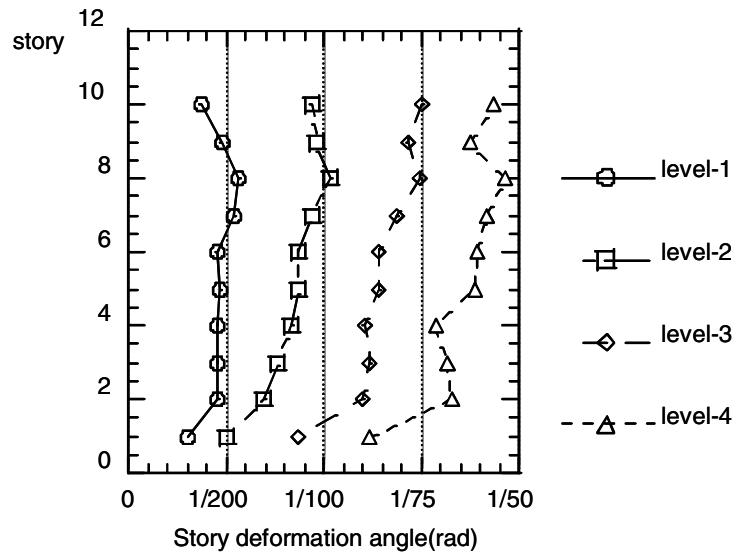


Figure 5. Story deformation angles

Strain induced in the beam-end by different levels of ground motion inputs

Table 7 shows a list of maximum ductility factors and cumulative ductility factors computed from the beam-end rotation angles in the individual ground motions at the level-3 and level-4 ground motion input. At the level-3 and level-4 ground motion inputs, plasticization is observed in all ground motion types, but the ductility factors remain below 1.5 up to the level-3 ground motion input.

Table 7. Ductility factors and cumulative ductility factors of beam end

Ground motion	Ductility factor		Cumulative ductility factor	
	L3	L4	L3	L4
elns	1.0	1.6	1.0	5.5
kobens	1.5	1.9	4.9	9.4
taftew	1.4	1.9	3.5	10.6
hatiew	1.2	1.9	3.5	7.1
center	1.4	2.2	4.9	18.7

Damper's maximum plastic deformation capacity

Table 8 shows a list of maximum ductility factors μ and cumulative ductility factors η for the dampers. It can be seen from the mean values of μ s and η s in the individual ground motion levels that η s are approximately 15-fold larger than μ s. The η s of the “center”, the simulated ground motions created by the Building Center of Japan, are larger compared to the other ground motions. This is considered to be due to the fact that the velocity response spectrum characteristically becomes constant in the long period range, hence, a given building structure is not affected by the variation of a natural period.

Table 8. Maximum values for μ and η of damper

Ground motion	μ				η			
	L1	L2	L3	L4	L1	L2	L3	L4
elns	3.4	6.6	10.8	16.1	34.9	99.9	161.	263.
kobens	4.0	8.5	12.9	16.2	28.2	74.4	144.	182.
taftew	3.7	8.3	13.4	16.9	37.5	95.8	171.	302.
hatiew	3.3	6.5	10.8	15.6	50.1	122.	180.	260.
center	3.3	6.1	11.7	16.7	92.9	154.	304.	451.
Mean	3.5	7.2	11.9	16.3	48.7	109.	192.	292.

Damper's cumulative plastic strain energy absorption capacity

Energy absorption rate ω ($=W_p/W_y$) is defined as a parameter that is found by: dividing the damper's cumulative plastic strain energy absorption W_p by W_y obtained by multiplying the damper's yield load by the damper's elastic-limit deformation, and non-dimensionalizing the results from the preceding calculation.

The maximum values for energy absorption rates ω in the individual ground motions are listed in Table 9. Although the energy absorption rate distribution has similarities with the cumulative ductility factor distribution at all input levels.

Table 9. Maximum values for ω of damper

Ground motion	ω			
	L1	L2	L3	L4
elns	20.2	84.0	179.	273.
kobens	21.8	88.8	177.	237.
taftew	21.1	88.2	185.	275.
hatiew	27.1	80.7	152.	220.
center	50.0	153.	346.	549.
Mean	28.0	98.9	208.	311.

PERFORMANCE EVALUATIONS

Ranking of total input energy

Energy equivalent velocities V_E (Akiyama [7]) computed from the total input energies obtained from the responses to the individual ground motion inputs are listed in Table 10. The V_E values vary from one ground motion level to the next. In this study, however, the mean value of the five ground motions taken by each input level is defined as the total input energy of the level. The V_E can also be estimated by using a given system's first-order natural period value in velocity response spectrum when the damping ratio is 2%.

Damper performance evaluation indexes

As damper performance evaluation indexes, this study adopts ductility factor (μ), cumulative ductility factor (η), and energy absorption rate (ω). In the performance evaluation of earthquake-resisting elements, approaches that adopt the ductility and cumulative ductility factors as evaluation indexes have conventionally been used in which only damage in the plastic region is a major target. For dampers, however, it has been pointed out that a comprehensive approach using the energy absorption rate is also necessary. In consideration of this fact, this study adopts the aforementioned three indexes. The relationships between the individual evaluation indexes and the energy equivalent velocities V_E are presented in Figure 6 along with digression equations. Taking 1.0 for the mean value of the individual evaluation indexes at the level-4 ground motion input, individual index values at the ground motion inputs of different levels are standardized and plotted on the longitudinal axis. The evaluation results indicate that the values of the three indexes μ , η , and ω increase linearly with increasing V_E values, although the gradient varies from one index to the next.

Table 10. Total input energies based on V_E

Ground motion	V_E (m/s)			
	L1	L2	L3	L4
elns	0.75	1.40	2.06	2.70
kobens	0.70	1.41	2.04	2.58
taftew	0.75	1.46	2.24	2.96
hatiew	0.91	1.54	2.08	2.63
center	1.14	1.98	2.95	3.84
Mean	0.85	1.56	2.27	2.94

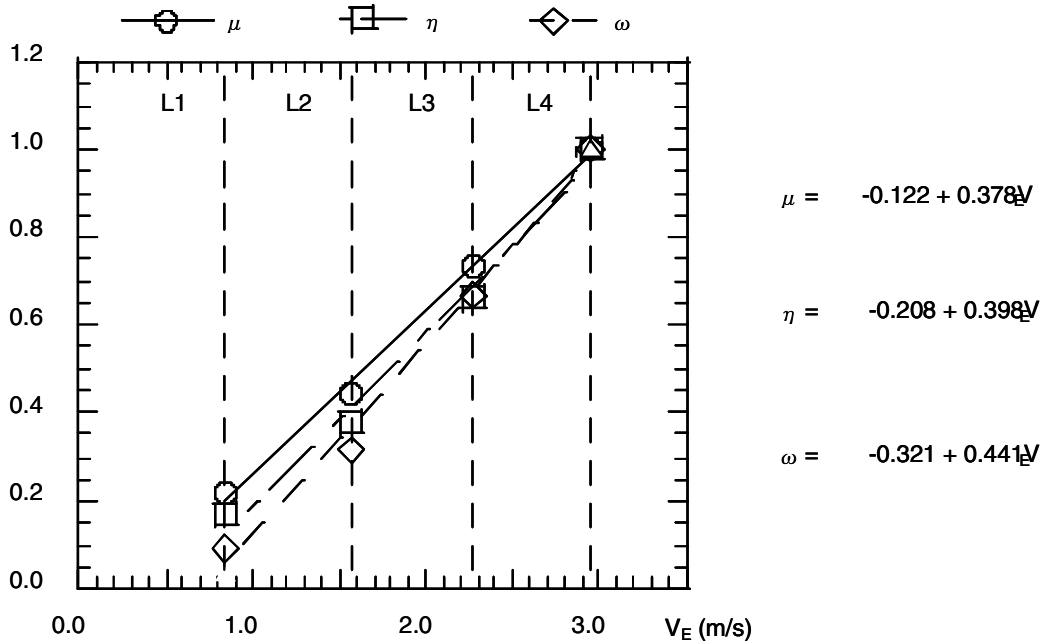


Figure 6. Damper performance evaluation indexes

Table 11. Results of testing

Specimen	Cyclic No.s	μ	η	ω
Type 1	3.0% 14	23.4	691.	1719.
Type 2	2.0% 2	15.6	178.	191.
Type 3	3.0% 1	23.4	240.	491.
Type 4	2.5% 1	17.9	191.	380.

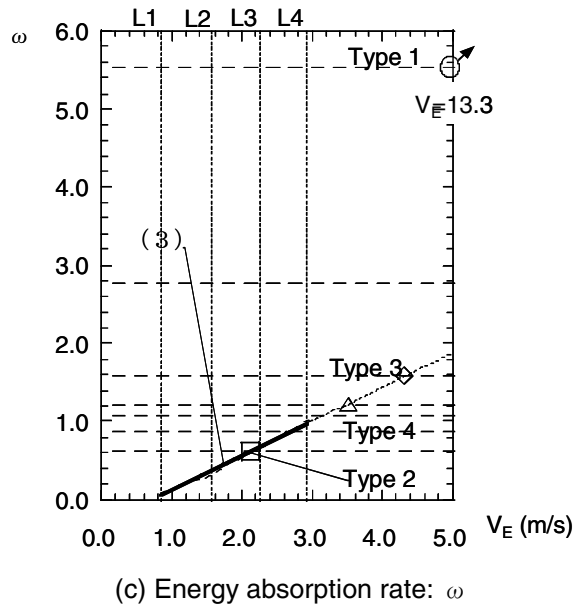
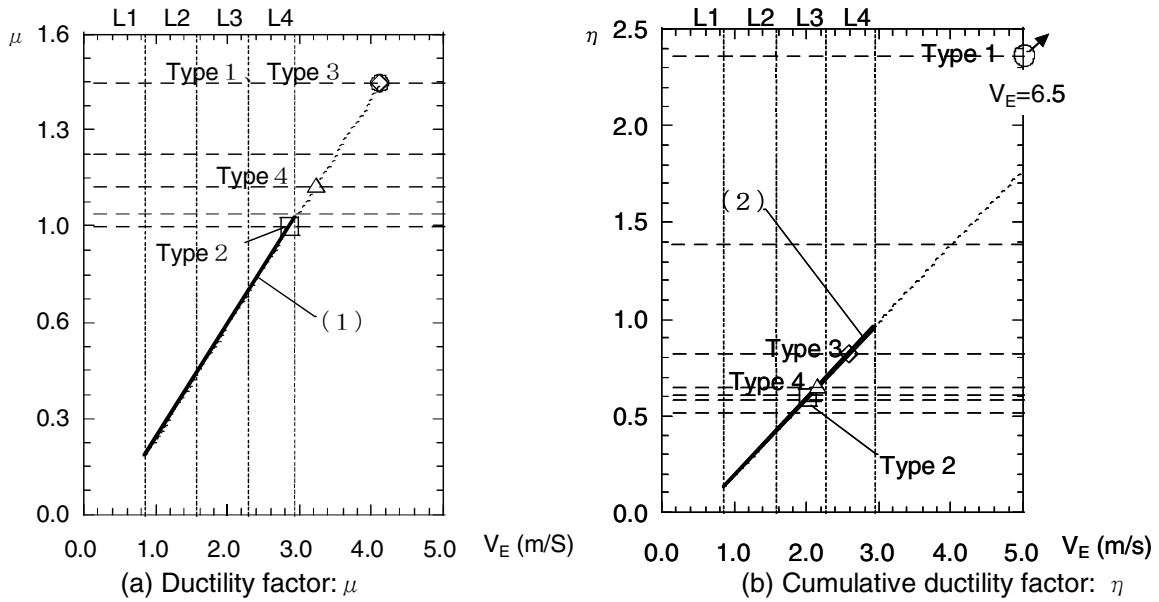


Figure 7. Performance evaluation indexes from testing results

Damper performance evaluation based on the testing results

This section discusses the correspondence between the findings obtained from the comparative performance testing of buckling restrained braces and those from the analysis performed in this study. The results from these tests are outlined in Table 11.

The testing results obtained from the individual specimens are standardized based on the mean values of the above mentioned three indexes at the level-4 ground motion input, and V_{ES} are computed from the digression equations presented in Figure 6.

Figure 7 shows the relations between the damper performance evaluation indexes of the individual specimens and V_{ES} . The extended application of the digression equations presented in Figure 7 to the ground motion levels exceeding 4 is possible as indicated by the dotted line. It can be seen from Figure 7 that, in each performance evaluation index, all the specimens meet the damper's performance criteria at the level-2 ground motion input. In consideration of the fact that ω permits more accurate evaluation of the damper's cumulative plastic deformation capacity compared to η , all the specimens excluding the Type 2 almost meet the damper's performance criteria at the ground motion input up to level-3, which is considered to be the damage limit level for the primary structure. Only one specimen, Type 1, meets the damper's performance criteria at the level-4 ground motion input. Specimen Type 3, however, also meets the requirements in terms of ω , and it is considered that this specimen almost meets the damper's performance criteria too at the level-4 ground motion input.

Focusing our attention on the evaluation results obtained from Type 1 and Type 3, cyclic loading with 3 percent strain amplitude has shown that these specimens have different levels of cumulative plastic deformation capacity. In each index, however, Specimen Type 1 has a safety margin approximately 2 to 10 times, larger than the damper's performance criteria at the level-4 ground motion input. Therefore it can be said that the specimen has performance higher than that required. Specimen Type 3 has a safety margin approximately 0.8 to 2 times larger than the performance criteria at the level-4 ground motion input, hence, it can also be said that this specimen meets the minimum performance criteria.

CONCLUSIONS

- (1) The author designed specimens demonstrating four types of commercially available buckling restrained braces, which are considered to resist buckling even at a story deformation angle of 1/100, based on the description in their references. The specimens were prepared under the same conditions and put to a test.
- (2) As was aimed at by the design, all specimens were empirically found to have sufficient hysteresis to withstand strains up to 1.0 percent.
- (3) Under high strains exceeding 1.0 percent, the four specimens exhibited significantly different performances due to their buckling restraining methods. Specimen Type 1, 3, 4 and 2 cumulatively absorbed greater amounts of energy in the listed order.
- (4) Specimens Type 2 and 4 having no unbonded material finally fractured as a result of tensile fracture caused by a rapid progress in local buckling. The unbonded material prevents the transmission of the axial force of the core plate to the restraining part. Furthermore, it is considered to keep a uniform clearance between the core plate and restraining part and prevent the occurrence of abrupt local buckling.
- (5) In the case of evaluation using three indexes, the ductility factor (μ), cumulative ductility factor (η), and energy absorption rate (ω), the degree of damage evaluated with μ , η , and ω tends to increase linearly.
- (6) All the specimens excluding the Type 2 almost meet the damper's performance criteria at the level-3 ground motion input. Only Specimen Type 1 meets the criteria of level-4.

ACKNOWLEDGMENT

The author wishes to thank Prof. A. Wada of Tokyo Institute of Technology for his advice in this study. The author also wishes to thank Dr. H. Ogawa, Mr. M. Murai of Kanagawa University and Mr. T. Kato of Alpha Structural Design for their cooperation in the performance of tests, compilation of experimental data and numerical analysis, and Dr. Y. H. Huang of Imbsen & Associates, Inc. for his assistance in creating an analytical program.

This study was undertaken as part of the research project of Typhoon and Earthquake-induced Disaster Control and Mitigation (TEDCOM).

REFERENCES

1. Wada A., Iwata, M., et al. "Damage-controlled design for buildings." Maruzen, 1998
2. Fujimoto M., Wada A, et al. "Unbonded brace encased in buckling-restraining concrete and tube." Structural Engineering, Vol. 34B, AIJ, 1988.
3. Kamiya M, Shimokawa H, et al. "Elasto-plastic behavior of flat-bar brace stiffened by square steel tube." Annual meeting of the AIJ, 1999.
4. Fukuda K., Ishibashi T, et al. "Seismic retrofit of over-track buildings using brace-type hysteretic dampers." Annual meeting of the AIJ, 1999
5. Suzuki N., Kono R, et al. "H-section steel brace encased in RC or steel tube." Annual meeting of the AIJ, 1994
6. Fujimoto M., Wada A., Iwata, M., et al. "Theory of one-dimensional members." Jikkyo, 1981
7. Akiyama H. "Seismic design of buildings based on energy balance." Gihodo, 1999